On the effect of an anisotropy-resolving subgrid-scale model on large eddy simulation predictions of turbulent open channel flow with wall roughness

Zhang, Yanrong
Department of Aeronautics and Astronautics, Kyushu University

Kihara, Hisashi
Department of Aeronautics and Astronautics, Faculty of Engineering, Kyushu University

ABE, Ken-ichi
Department of Aeronautics and Astronautics, Faculty of Engineering, Kyushu University : Professor

出版情報：Journal of Turbulence. 18 (9), pp.809-824, 2017-06-05. Taylor and Francis
バージョン：
権利関係：

On the effect of an anisotropy-resolving subgrid-scale model on large eddy simulation predictions of turbulent open channel flow with wall roughness

Yanrong Zhang[a)*], Hisashi Kihara[b)], Ken-ichi Abe[c)]

Department of Aeronautics and Astronautics, Kyushu University, 744 Motooka, Nishi-ku, Fukuoka, 819-0395, Japan, TEL 092-802-3024,

[a]*yanrongz87@gmail.com*

[b]*kihara@aero.kyushu-u.ac.jp*

[c]*abe@aero.kyushu-u.ac.jp*

Abstract – A large eddy simulation (LES) was conducted of turbulent flow in a channel with a rough wall on one side and a free surface on the other side by adopting an anisotropy-resolving subgrid-scale (SGS) model. A shear Reynolds number of $Re_\tau = 395$ was used based on the mean friction velocity and channel height. To investigate the grid dependency of the LES results caused by the SGS model, three grid resolutions were tested under the same definition of a roughness shape by using the immersed boundary method. The results obtained were compared with direct numerical simulation data with and without the wall roughness. For comparison with the same test cases, LES without the extra anisotropic term were also performed. The primary focus was on how the present anisotropic SGS model with coarser grid resolutions can properly provide the effects of roughness on the mean velocity and turbulent stresses, leading to a considerable reduction of the computational cost of LES.

Keywords: anisotropy-resolving SGS model, channel flow, roughness, immersed boundary method.

1. Introduction

Turbulent flow in a channel with surface roughness is very common in many engineering applications. Besides roughness brought by structures or materials, vapor bubbles that are attached to the wall in subcooled flow boiling can also resemble near-hemispherical roughness elements [1]. A flow over a rough wall can be divided into two parts: an inner layer that is directly affected by the roughness elements, and an outer layer that is away from the wall. Different shapes or distributions of an element may bring various influences on turbulence features from the near-wall region to the central flow. To date, abundant numerical and experimental results are available concerning this issue, as presented in the following for examples.

Direct numerical simulation (DNS) of turbulent incompressible flow in a plane channel with one of its walls covered with regular three-dimensional roughness elements (called ‘egg carton’-shaped surface) was performed by Bhaganagar et al. [2]. From the results, significant differences in processes associated with the wall-normal fluxes of the Reynolds shear stress and turbulence energy were demonstrated using the higher-order moments and the energy budgets between the smooth-wall and rough-wall sides. Chatzikyriakou et al. [1] performed numerical simulations of turbulent channel flow with smooth walls and walls featuring rough hemispherical elements using both DNS and large eddy simulation (LES). In their research, a parametric study was conducted including the effect of shear Reynolds number, normalized

roughness height and relative roughness spacing. The effect of the distribution pattern (regular square lattice vs. random pattern) of these rough elements on the walls was also verified. Shamloo et al. [3] analyzed the effects of roughness density and flow submergence on the flow features in open channel using LES. Jin et al. [4] used both a finite volume method and a Lattice Boltzmann method to determine the detailed structure of turbulent flow through channels with smooth and rough walls. Marchis and Napoli [5] investigated the effects of irregular 2D and 3D roughness on the turbulence by performing a wall-resolved LES of fully developed turbulent channel flows over two different rough surfaces. In their research, the roughness function obtained with 3D roughness is larger than that with a 2D one for the same mean height. Andersson et al. [6] investigated the validity in assuming the roughness can be represented by a numerical model through performing Reynolds-averaged Navier-Stokes simulations over a surface with a large roughness, and showed the importance of an appropriate surface description. Bailon-Cuba et al. [7] performed DNS of a turbulent channel flow with 2D wedges of random height on the bottom wall. A DNS study of channel flow with rough walls comprising staggered arrays of cubes was presented by Leonardi and Castro [8]. Nagano et al. [9] performed a DNS of heat transfer in turbulent channel flows with transverse-rib roughness to determine the effects of roughness on the statistical quantities of the velocity and thermal fields.

An experimental study of fully developed turbulent channel flow and an adverse pressure gradient turbulent channel flow over smooth and rough walls comprising two-dimensional square ribs was performed by Tsikata and Tachie [10]. Schultz and Flack [11] presented experimental measurements for roughness-wall boundary layers covering a Reynolds-number range from hydraulically smooth to fully rough flow regimes. Keirsbulck et al. [12] investigated the effect of roughness wall in a zero pressure-gradient turbulent boundary layer using hot-wire anemometry. Communication between the wall region and the outer region of a turbulent boundary layer was shown to be present. The experimental evidence provided by Krogstad and Antonia [13] indicated that the surface geometry significantly affects the turbulent characteristics of the flow, although the two rough surfaces were designed to have nominally the same effect on the mean velocity profile.

LES is well known as a useful way to predict turbulent flow. When LES is applied, the grid-scale (GS) eddies are directly resolved and the SGS eddies need to be modeled. The most widely used SGS model is the Smagorinsky model [14]. In order to overcome the drawback of the Smagorinsky model, Germano et al. [15] proposed an SGS eddy viscosity model in which a single universal coefficient is replaced by a dynamically computed value. The model coefficient was yielded based on the stresses obtained by the grid and test filters using the same concept of the Smagorinsky model for the anisotropic parts of SGS stresses. The method of evaluating the model coefficient was modified by Lilly [16] using a least-square approach. Zang et al. [17] modified the base model in [15] by employing the mixed model of Bardina et al. [18], in which the modified Leonard term was explicitly calculated in the modified model, leading to much smaller model coefficient being obtained. Vreman et al. [19] proposed a modification of the turbulent stress expression using alterative filter definition in the above dynamic mixed model [17] for more strict mathematical consistency. Recently, with a different perspective, an anisotropy-resolving subgrid-scale (SGS) model for LES was proposed by Abe [20]. In this model, the SGS-stress expression is constructed by combining an isotropic eddy-viscosity model with an extra anisotropic term (EAT). Applying the model to several fundamental test cases indicated the basic capability of this SGS modeling concept, particularly for coarser grid-resolutions. If this model also works well for predicting turbulent wall-shear flows with wall roughness, a considerable reduction in computational cost for LES is expected.

Hence, in the present study, an LES of turbulent flow in a channel, with a rough wall on

one side and a free surface on the other, was performed by adopting this anisotropy-resolving SGS model of Abe [20]. The primary concern of this study is how the present anisotropic SGS model can detail properly the effects of roughness on the mean velocity and turbulent stresses for coarser grid resolutions. The results obtained are compared with those of DNSs for both smooth and rough walls. The present DNSs are first validated using another reference DNS data for the smooth case. To investigate the grid dependency of the LES results resulting from the present SGS model for turbulence with wall roughness, three grid resolutions are tested for the above open plane channel flow under the same definition of roughness configuration. In this study, the immersed boundary method is used to define the roughness placed on the bottom surface. A detailed description of the turbulence model adopted for this study is given in Section 2. The computational conditions and roughness model are introduced in Section 3. A discussion of the results is presented in Section 4. Finally, some conclusions are summarized in Section 5.

2. Turbulence model

The governing equations of LES for incompressible flow can be written as

$$\frac{\partial \bar{U}_i}{\partial x_i} = 0, \quad \frac{D\bar{U}_i}{Dt} = -\frac{1}{\rho}\frac{\partial \bar{P}}{\partial x_i} + \frac{\partial}{\partial x_j}\{\nu\left(\frac{\partial \bar{U}_i}{\partial x_j} + \frac{\partial \bar{U}_j}{\partial x_i}\right) - \tau_{ij}\}, \tag{1}$$

where $\overline{(..)}$ denotes a filtered value, and ρ, $\bar{P}$, $\bar{U}_\iota$ and ν denote density, filtered static pressure, filtered velocity and kinematic viscosity, respectively. Note that since incompressible flow is considered, the viscous term can also be written as $\nu\frac{\partial^2 \bar{U}_i}{\partial x_j \partial x_j}$. The SGS-stress tensor τ_{ij} is defined as $\tau_{ij} = \overline{U_\iota U_J} - \bar{U}_\iota \bar{U}_J$. For modeling τ_{ij}, a linear eddy-viscosity model (EVM), that is often used, takes the canonical form

$$\tau_{ij}^a = -2\nu_{SGS}S_{ij}, \quad S_{ij} = \frac{1}{2}(\frac{\partial \bar{U}_i}{\partial x_j} + \frac{\partial \bar{U}_j}{\partial x_i}), \tag{2}$$

where S_{ij} denotes the resolved strain-rate tensor, and $\tau_{ij}^a = \tau_{ij} - \tau_{kk}\delta_{ij}/3$. In the present simulations, an SGS-stress model is constructed by combining a representative isotropic EVM with an EAT proposed by Abe [20]. Its basic formulation is as follows,

$$\tau_{ij} = \frac{2}{3}k_{SGS}\delta_{ij} - 2\nu_{SGS}S_{ij} + 2k_{SGS}b_{ij}^{SGS}, \tag{3}$$

where the anisotropy tensor b_{ij}^{SGS} is defined as

$$b_{ij}^{SGS} = \frac{\tau'_{ij} - (-2\nu' S_{ij})}{\tau'_{kk} - (-2\nu' S_{kk})} - \frac{1}{3}\delta_{ij} = \frac{R'_{ij}}{\tau'_{kk}} \tag{4}$$

with $\tau'_{ij} = C_B(\bar{U}_i - \widehat{\bar{U}}_i)(\bar{U}_j - \widehat{\bar{U}}_j)$, a well-known 'scale-similarity model' proposed by Bardina et al. [21]; $\widehat{(..)}$ denotes the test-filtering operator. The equivalent eddy viscosity is modeled as

$$\nu' = -\tau_{ij}'^{a} S_{ij}/(2S_{mn}S_{mn}), \tag{5}$$

where $\tau_{ij}'^{a} = \tau_{ij}' - \tau_{kk}'\delta_{ij}/3$. In Eq. (4), $R_{ij}' = \tau_{ij}'^{a} - (-2\nu' S_{ij})$ is a 'SGS-stress anisotropy term' that is evaluated by subtracting an EVM form from the original Bardina model. In Eq. (3), $k_{SGS} = \tau_{kk}/2$ is the SGS turbulent kinetic energy, and the SGS viscosity ν_{SGS} is modeled as

$$\nu_{SGS} = C_{SGS} f_{SGS} \sqrt{k_{SGS}}\Delta, \qquad f_{SGS} = 1 - \exp\{-(\tfrac{y_\varepsilon'}{A_0})^{4/3}\}. \tag{6}$$

The constants of the model C_{SGS} and A_0 are set to $C_{SGS} = 0.05$ and $A_0 = 30$. The SGS filter width Δ is defined as

$$\Delta = \sqrt{the\ maximum\ area\ among\ the\ faces\ of\ a\ cell}; \tag{7}$$

in a Cartesian-structured grid system, it becomes

$$\Delta = \sqrt{\max(\Delta_x\Delta_y, \Delta_y\Delta_z, \Delta_z\Delta_x)}. \tag{8}$$

For the model function f_{SGS}, the wall-distance parameter y_ε' is modeled as $y_\varepsilon' = \left(\frac{u_\varepsilon y}{\nu}\right)\sqrt{C_l \frac{y}{\Delta}}$ with $C_l = 4$, where $u_\varepsilon = (\nu\varepsilon_{SGS})^{1/4}$ and $\varepsilon_{SGS} = C_\varepsilon \frac{k_{SGS}^{3/2}}{\Delta} + \frac{2\nu k_{SGS}}{y^2}$ with $C_\varepsilon = 0.835$. The SGS turbulent kinetic energy k_{SGS} is determined from the usual form of the transport equation using

$$\frac{Dk_{SGS}}{Dt} = \frac{\partial}{\partial x_j}\left\{\left(\nu + C_k f_{SGS}\sqrt{k_{SGS}}\Delta\right)\frac{\partial k_{SGS}}{\partial x_j}\right\} - \tau_{ij}\frac{\partial \bar{U}_i}{\partial x_j} - \varepsilon_{SGS}, \tag{9}$$

and setting $C_k = 0.1$.

3. Computational conditions and roughness model

In the present study, we adopted a two-dimensional open channel-flow configuration as the test case, where one of the surfaces is a no-slip wall with/without roughness and the other is a free surface. Several studies of this kind adopted a channel-flow configuration with a rough wall on one side and a flat wall on the other side. However, this configuration greatly affects the balance of the wall-shear stress on each surface, resulting in a considerable shift in the center position of the mean velocity profile. Because this balance also depends on the performance of the SGS model as well as the grid resolution, the point of issue may become obscure. This is the main reason why the aforementioned open-channel configuration was adopted in this study, as the whole wall-shear stress must be covered by the rough wall and the position of maximum mean-velocity must reside on the free surface. Therefore, the point of issue in this study, the predictive performance of the SGS model for different grid resolutions, can be focused on properly.

In this simulation, the periodic boundary condition is specified in the streamwise and spanwise directions. To investigate the grid dependence arising from the present SGS model, three Cartesian-structured grids are made with the same computational domain of $4.8\delta \times \delta \times 2.4\delta$ in x-, y-, and z-directions, respectively (Table 1). The Reynolds number based on the

mean friction velocity u_τ and the open-channel height δ is set to 395 for all test cases. First, two simulations without roughness (i.e., a smooth wall) are performed, where DNS is performed for a fine grid and LES is performed for a coarse grid. The data obtained are used to validate the present simulation by comparing with the corresponding DNS data from a previous study [22]. Although the reference DNS was performed for a plane channel flow, it is expected that the fundamental features in the near-wall region are similar to those of the present simulation (see Section 4).

In this study, the direct forcing approach of the immersed boundary method is employed to build the roughness structure, in which a body force is added to the flow field where the roughness locates to express the influence of rough elements. The validation (not shown here) of the present direct forcing program for static as well as moving boundary has been performed by Hirose et al. [23]. The bottom surface is configured with a surface roughness defined using the 'egg-carton' shaped-surface function $\sigma(\mathrm{x},\mathrm{z})$ introduced in Bhaganagar et al. [2],

$$\sigma(\mathrm{x},\mathrm{z}) = \sigma_0 + \frac{h}{4}\left[-1 + \left(1 + \sin\left(\frac{2\pi x}{l_x} + \frac{2\pi z}{l_z}\right)\right) \times \left(1 + \sin\left(\frac{2\pi x}{l_x} - \frac{2\pi z}{l_z}\right)\right)\right], \tag{10}$$

where h is the roughness height from peak to valley, σ_0 is mean offset, l_x and l_z are streamwise and spanwise wavelengths of the roughness elements, the parameters are now set as $h = 0.0506329\delta$ ($h^+ = \frac{hu_\tau}{\nu} = 20$), $\sigma_0 = \frac{h}{4}$, $l_x = 0.6\delta$, and $l_z = 0.3\delta$. According to the results employing minimal-span channels by Chung et al. [24], the scale of the present channel with the above roughness setting is believed sufficient to catch the flow properties such as mean velocity and turbulence stresses.

An open-CFD-code 'FrontFlow/Red' [25] is used in the present study. This code adopts an unstructured finite-volume procedure with vertex-centered type storage on a grid. The second-order central difference scheme is used to discretize the spatial derivatives, except for the convection term of the transport equation of k_{SGS}, which was discretized by the second-order upwind scheme. Time marching is based on the fractional step method, in which the second-order Crank-Nicolson scheme is used for the velocity equations. Concerning the transport equation for k_{SGS}, the first-order Euler implicit scheme is used. The coupling of the velocity and pressure fields is based on the SMAC method. Note that our previous studies [20, 26] had investigated the effects of a first-order time-marching scheme and a second-order upwind scheme adopted for the transport equation of k_{SGS}. These investigations confirmed that the time-integration and space-discretization schemes used here did not have any crucial effect on the computational results. More detailed descriptions of the computational schemes are given in Abe [20].

In addition to the simulations using the aforementioned anisotropic SGS model, the present study conducted simulations using an isotropic eddy-viscosity type of SGS model without an EAT, which is actually composed of only the first two terms on the right-hand side of Eq. (3). From a comparison of the results obtained by these two SGS models, we can analyze the effects of the EAT on the predictive performance for this kind of turbulent flow with wall roughness.

Table 1: Grids for the three test resolutions with roughness.

	Coarse	Medium	Fine
$N_x \times N_y \times N_z$	$65 \times 121 \times 65$	$129 \times 121 \times 129$	$257 \times 121 \times 257$
Δx^+	29.6	14.8	7.4
Δy^+	1.2 - 4.5	1.2 - 4.5	1.2 - 4.5
Δz^+	14.8	7.4	3.7

Figure 1 depicts a grid as well as a configuration of roughness for the bottom surface. The rough-wall elements composing the bottom surfaces as defined by Eq. (10) are presented for comparison in Fig. 2. Even with the same functional definition, the three roughness configurations are somewhat different. As the grid coarsens, an obvious deviation from the 'egg-carton' profile appears, as evident in the coarse grid. This feature arises from the immersed boundary method used for building the roughness configuration. In the present study, the roughness is composed of small blocks of the same size as the corresponding local grid units in generating a discretized approximate structure of the 'egg-carton' surface. As a result, the coarse grid brings obvious large steps into the rough surface, which may look a little different from the original shape. The influence brought by this deviation is discussed in Section 4.

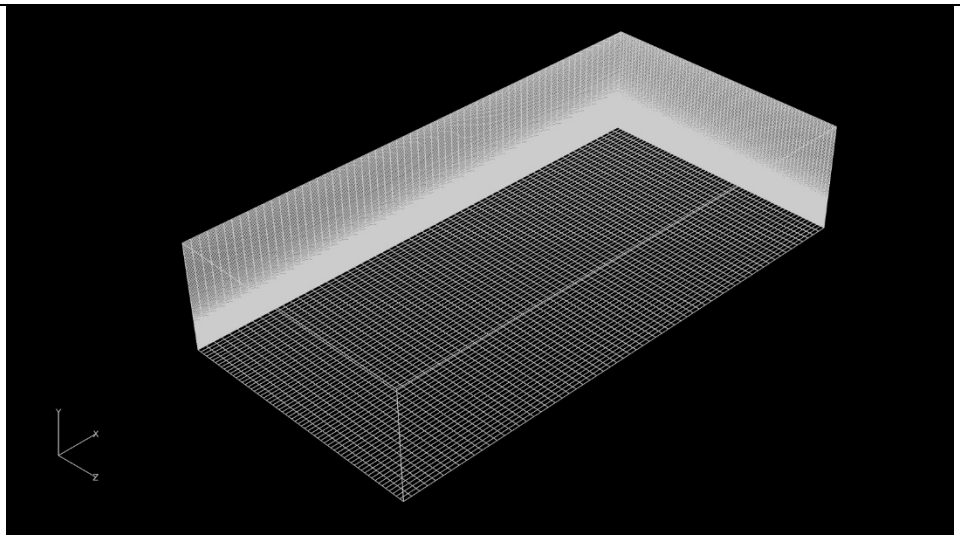

Grid

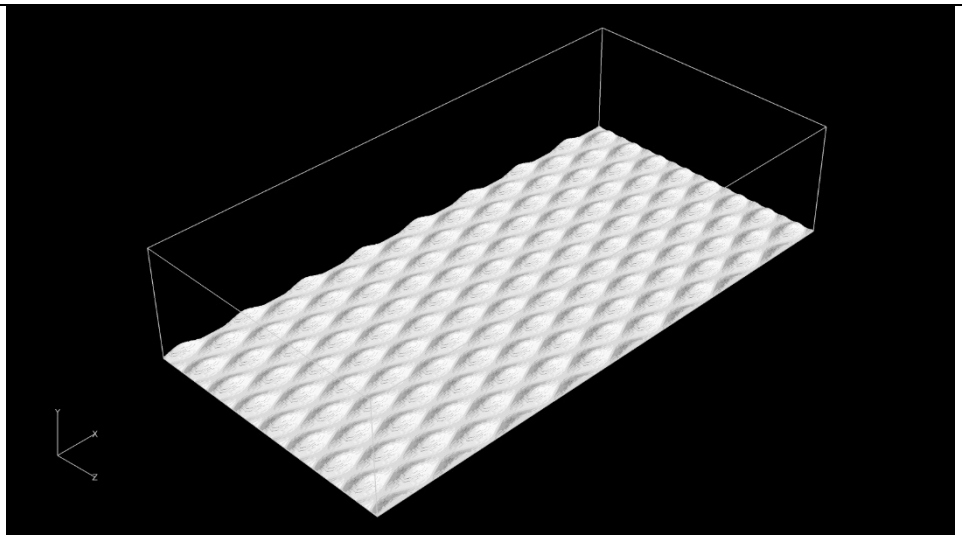

Roughness

Figure 1: Grid (coarse) and roughness (fine)

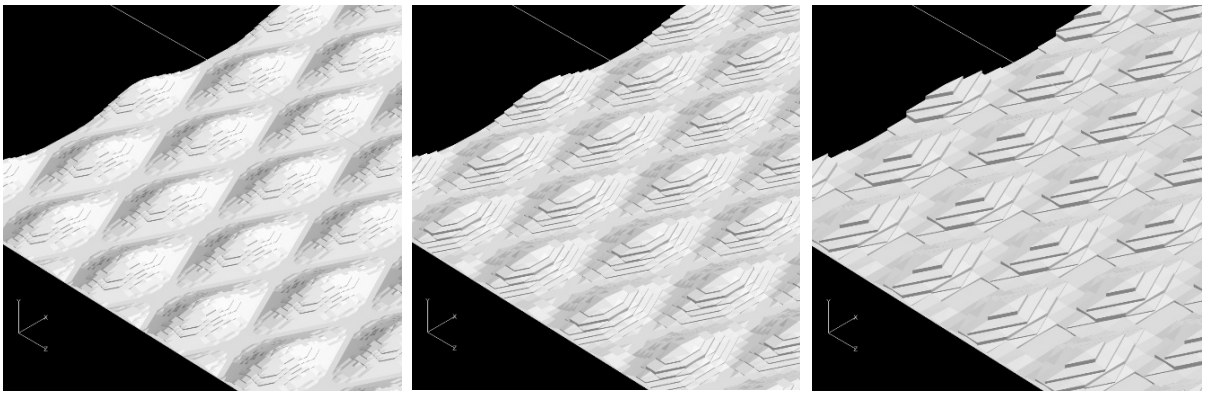

Fine **Medium** **Coarse**

Figure 2: Close-up views of the three rough bottom surfaces

4. Results and discussion

The basic performance of the present SGS model for a smooth wall has been validated in a previous study by Abe [20]. However, the present study adopts a different flow configuration, where one of the surfaces is treated as shear free. Therefore, to confirm the validity of the present simulation for the near-wall region on the bottom surface, Fig. 3 compares the mean streamwise velocity obtained by the DNS for a smooth wall and fine grid (Table 1) with the DNS results for a conventional channel flow reported by Moser et al. [22]. Note that to confirm the basic performance of the present SGS model for coarse grid resolution, the results of the LES with coarse grid (Table 1) are also included. It is found from Fig. 3 that the present DNS data correspond well to those by Moser et al. [22]. Moreover, even the LES with coarse grid yields satisfactory predictions for the mean streamwise velocity, although a slight difference is still observed.

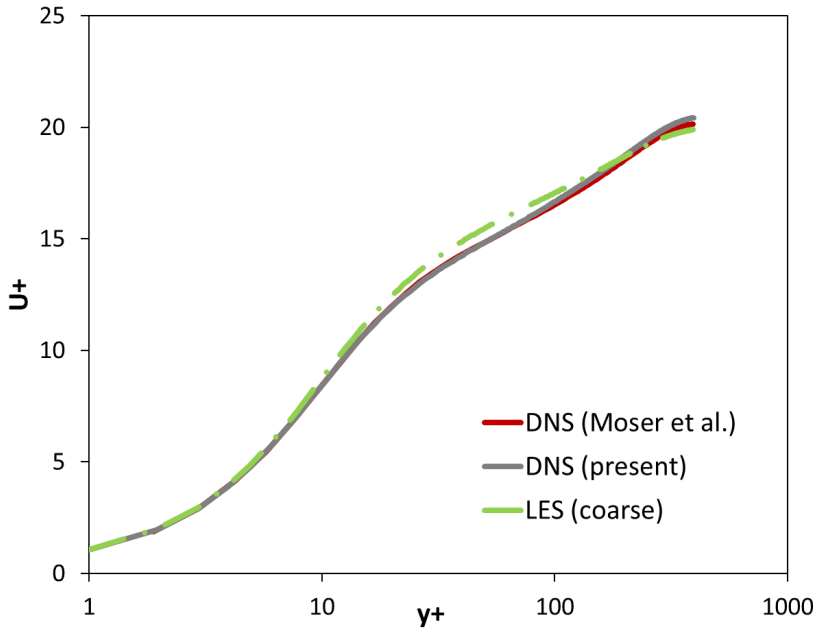

Figure 3: Mean streamwise velocity for the smooth wall

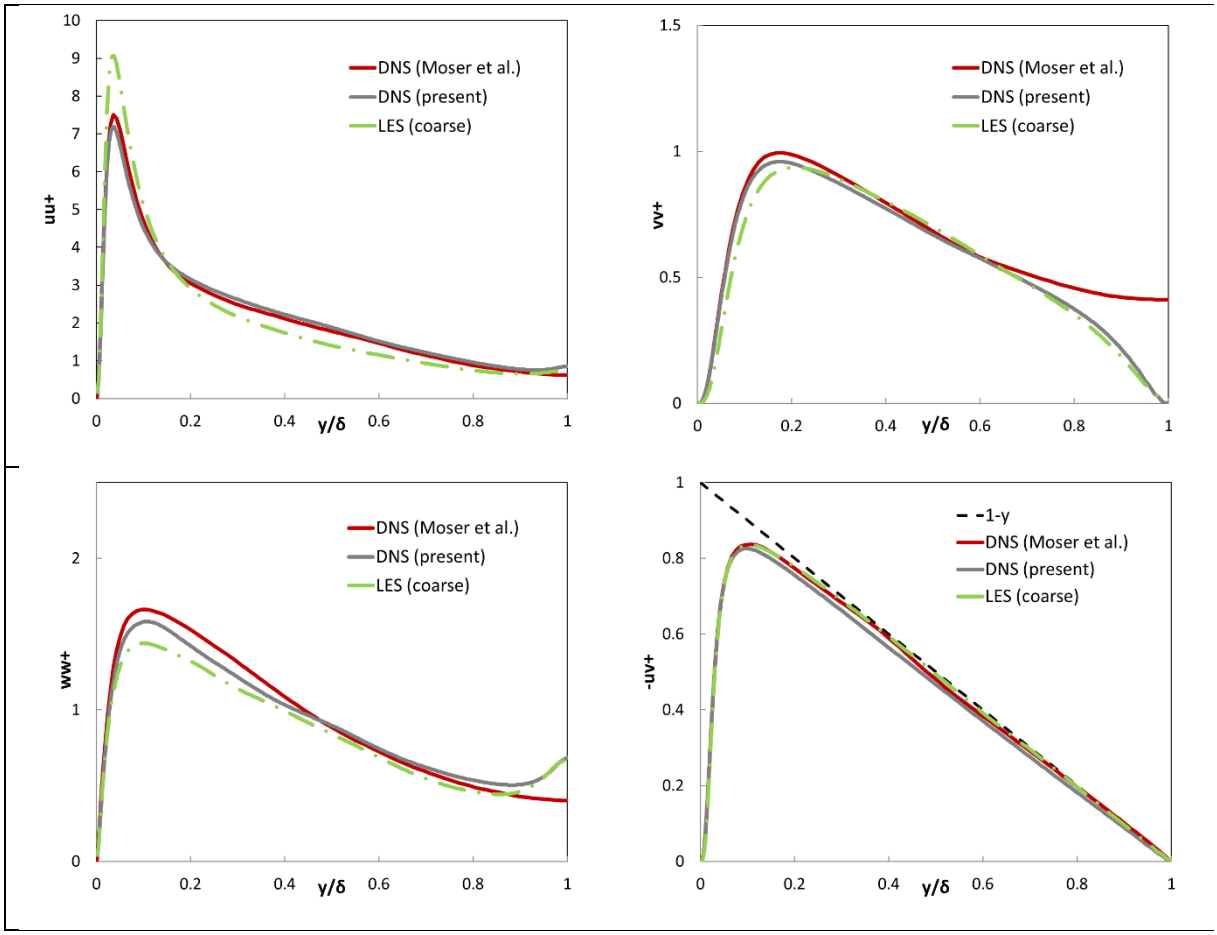

Figure 4: Comparison of Reynolds stresses for flow along a smooth wall

The normal components of the Reynolds normal stresses as well as the Reynolds shear stress are compared in Fig. 4. The results for both show generally good agreement in the region close to the no-slip wall on the bottom. Although there are considerable differences between the two DNS data in the upper region close to the free surface (center line in the reference DNS), no crucial effect is evident in the predictive performance on the bottom side, which is the main concern in this study. It is also notable that even the predicted Reynolds stresses near the free surface correspond well to what is generally known of this kind of flow. Concerning the LES with coarse grid, the belief is that generally reasonable results are obtained, although slightly higher streamwise and lower spanwise predictions are still seen in the near-wall region compared with the DNS data. Concerning the contribution of each term in Eq. (3), according to the analysis in [26] on the results of the channel flow case, the time-averaged SGS stresses calculated with the linear EVM term ($-2\upsilon_{SGS}S_{ij}$) mainly contributes to the SGS shear stress while its effect is very small for normal stresses. In contrast the EAT ($2k_{SGS}b_{ij}^{SGS}$) plays a dominant role for them.

The mean-velocity distributions for the three test cases with wall roughness are compared in Fig. 5, along with the DNS data for smooth and rough walls with free surface for reference as well as the LES data for a rough wall using the same grids without the EAT (i.e., isotropic SGS model) for added comparison. The DNS for rough wall was performed using the grid of $N_x \times N_y \times N_z = 385 \times 181 \times 385$ ($\Delta x^+ = 4.9$, $0.8 \leq \Delta y^+ \leq 4.0$, $\Delta z^+ = 2.5$) with the same domain as well as the boundary conditions for the present LES cases. Generally, for the

result of the DNS with roughness, the velocity profiles with wall roughness shift downward compared with that obtained in the smooth-wall DNS, but retain similar slopes, which corresponds to the general knowledge. For the LES results, the velocity profiles of the fine and medium cases with and without EAT generally agree well with the DNS data, while less downward shift is shown for the coarse cases. Note that this may arise as an effect of the quality of reproduction of the roughness configuration as well as the grid dependency of the SGS models. By comparing the results between LESs with EAT (i.e., anisotropic SGS model) and without EAT (i.e., isotropic SGS model) in the figure, for the fine and medium grid cases, the two models yield close profiles, while a difference is seen for the coarse grid case compared with the other two. Even considering the effect of the distortion of the roughness configuration that is shown below, an obviously better performance is obtained by adopting the SGS model with EAT than that without EAT, especially in the region exhibiting the logarithmic law, although both of them show some change in shape of the region. The isotropic SGS model without EAT shows a much larger discrepancy from the DNS data compared with the anisotropic SGS model with EAT. This fact indicates that the EAT contributes by reducing the grid dependency of the predictions, even for near-wall turbulence with wall roughness. The modification ΔU^+ from roughness effects is often called the roughness function. In the present study, it is evaluated to be about 3.0 as can be seen in Fig. 5.

To illustrate the effect of the roughness configuration reproduced by the immersed boundary method, the instantaneous velocity-vector plots obtained from the results with EAT as well as the roughness configurations generated for each case are shown in Fig. 6. As mentioned in Section 3, the roughness is composed of small blocks of the same size with corresponding local grid units. Therefore, in the finer grid case, a better shape of 'egg carton' surface can be realized. The distortion is more obvious with the coarse grid; not only is the rough surface modified with bigger stages, but also the height of the roughness peak decreases more significantly than with the fine or medium grid. This may be one reason for the lower roughness function ΔU^+ seen in Fig. 5. However, even considering this effect of shape distortion, the downshift of the profile of the coarse case without EAT is still underestimated, which is more likely caused by a higher grid dependency. The results also indicate that there is a low velocity region on the rear side of the rough mountain, while no obvious recirculation is observed in the present three test cases.

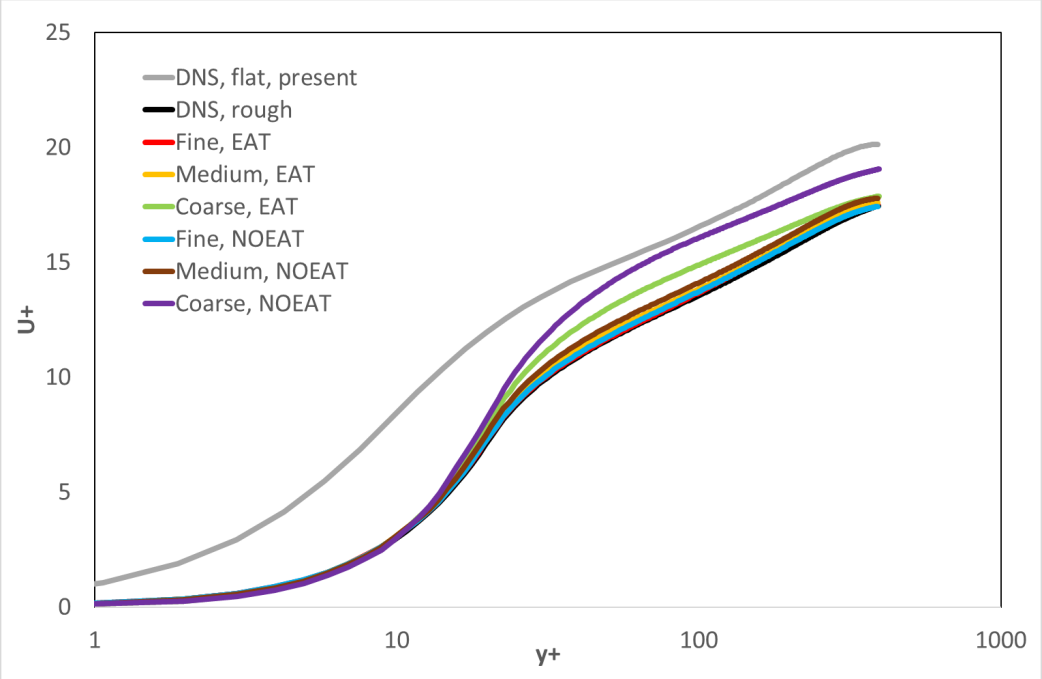

Figure 5: Comparison of the mean streamwise velocity for rough-wall cases with smooth-wall DNS

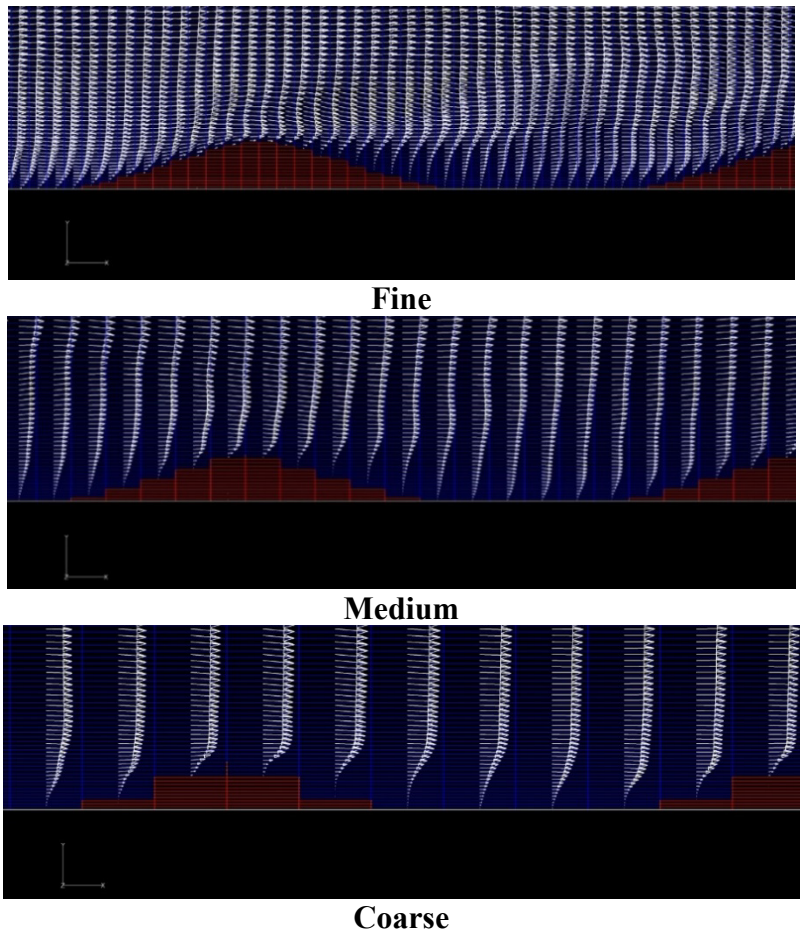

Figure 6: Instantaneous velocity with roughness shape at z=0 (with EAT)

From the distributions of turbulence energy shown in Fig. 7, the results of the DNS with roughness exhibit a lower peak compared with the DNS without roughness, and the location of the peak value is shifted away from the wall. The results of fine cases with and without EAT agree well with the DNS data . The profile of the medium case without EAT shows a slightly higher peak, while lower value can be seen in the outer layer that is similar to that with EAT. Obviously higher peak values are obtained in the coarse grid for both LES cases in the near-wall region, even higher than that in smooth DNS, the prediction is better for that with EAT than without EAT. In the outer layer, lower energy is obtained for both coarse cases, and even lower value is shown for the case with EAT .

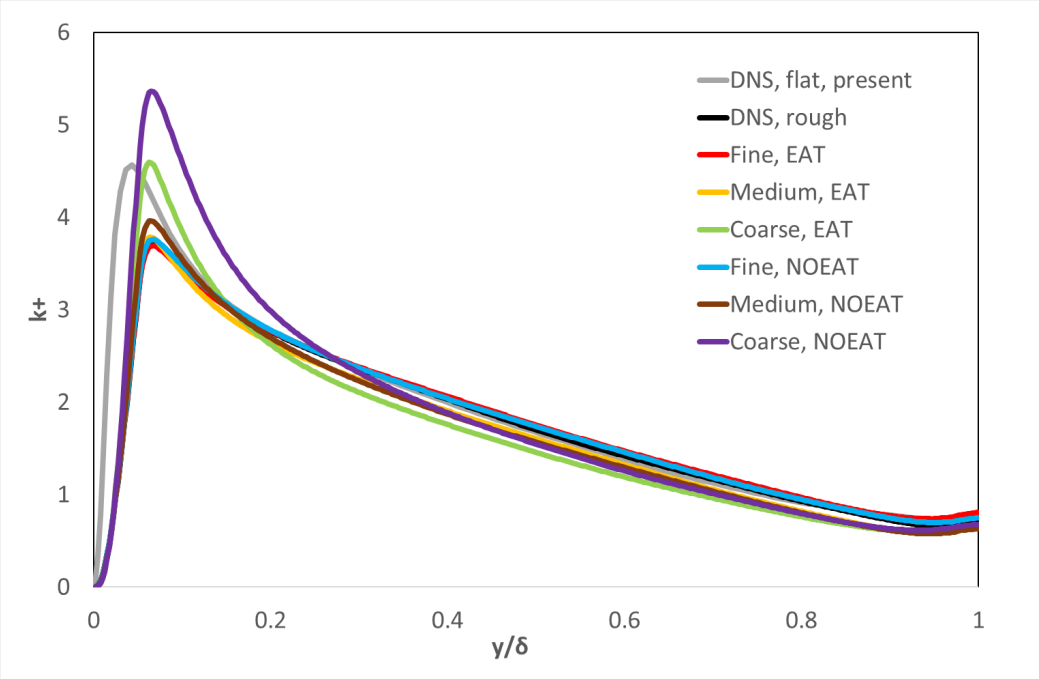

Figure 7: Comparison of turbulence energy distributions

The Reynolds normal stresses as well as the Reynolds shear stress for the rough-wall LESs are compared with each other, as well as with those of the smooth-wall and rough-wall DNSs in Fig. 8. As is found by comparing the rough-wall and smooth-wall DNS results, the roughness causes obviously lower peak for the streamwise component as well as a shift away from the wall for all the components. The results of fine cases with and without EAT agree well with that of DNS data . For the cases with EAT using the coarse grid, a higher peak value can be seen in the streamwise stress, whereas the peak values decrease in the wall-normal and spanwise directions, as found by comparing with the DNS results. This may be caused by a general feature of LES that coarse grid resolutions produce a stronger anisotropy. Moreover, the location of the peak value slightly changes in the wall-normal direction, which is likely to move farther away from the wall than with the fine and medium grids. Comparing with rough-wall DNS result, the departure mode with the coarse grid is similar to that for the smooth-wall cases when comparing LES and DNS profiles (Fig. 4), which implies that the exist of the roughness may not obviously influence the performance of the present SGS model on turbulence stresses, although the peak value decreases more apparently in the rough wall case. By comparing the cases with and without EAT, the fine and medium grids generally agree well with each other,

although slightly lower peak values are shown for the medium case with EAT than that without EAT in normal stress components. The difference in peak values are more obvious for the coarse cases, which indicates that the exist of EAT tends to cause lower normal stresses when the grid gets coarser in the present study.. This may lead to giving a higher peak value of the turbulence energy in the results without EAT.

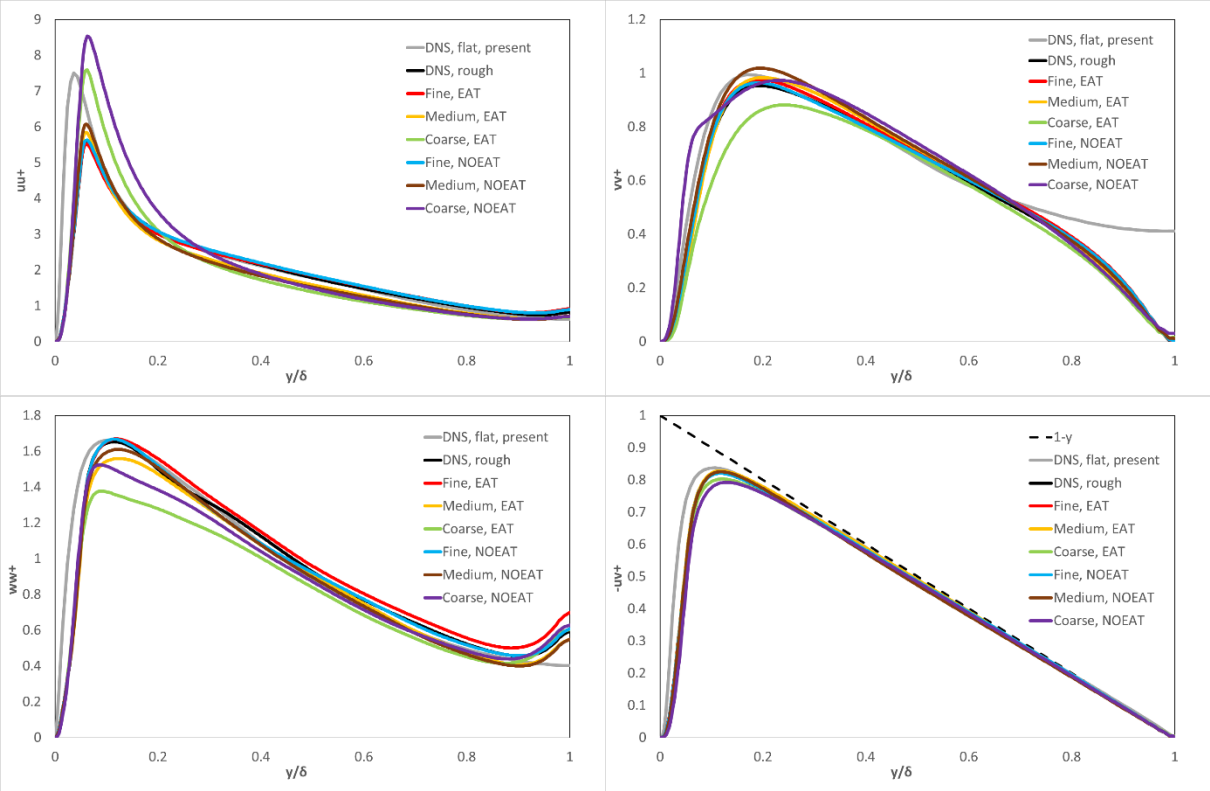

Figure 8: Comparison of Reynolds stress for the rough-wall cases and DNS cases (smooth and rough)

To investigate the effect of the SGS stresses on the total values, Fig. 9 shows the SGS components with and without EAT for the coarse grid case. It is found that the model with EAT successfully provides the SGS-stress anisotropy, while the model without EAT returns isotopic distributions. This is a notable feature of the present anisotropic SGS model. An important issue can be seen in the prediction in the wall-normal direction, where the model with EAT shows the correct wall-limiting behavior, while the model without EAT shows wrong one. This wrong behavior gives a considerable overprediction of the wall-normal component, leading to a decrease of the prediction accuracy for the total value of the wall-normal Reynolds stress. Concerning the SGS shear stress, similar profiles are obtained for both models, although there can be seen a slight difference in shape. Such being the case, it is confirmed that the EAT contributes to improving the distributions of the SGS stresses, resulting in better predictions of the total stress components.

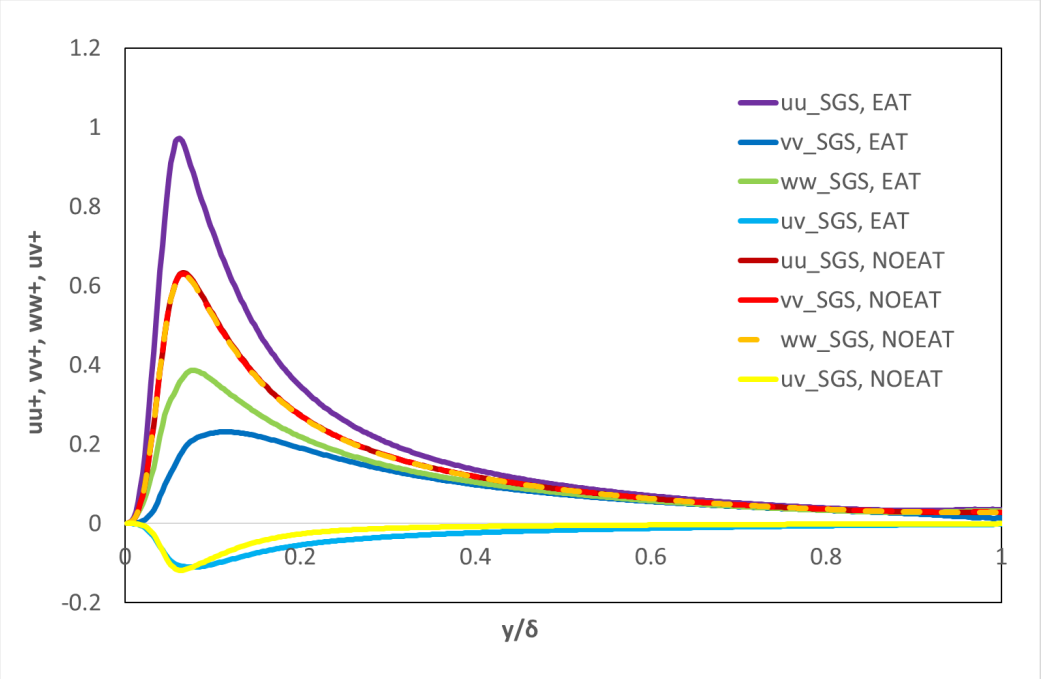

Figure 9: SGS components of the Reynolds stresses for the coarse case.

From the results for the instantaneous vortex structures and streamwise velocity contours of rough-wall cases with EAT as well as those for the smooth-wall and rough-wall DNSs (Fig. 10), the vortex structures for the coarse grid show a slightly different aspect from the fine and medium grids under a certain contour parameter for plotting, whereas the latter two are similar to each other, as well as the rough-wall DNS results. For the fine and medium grids, more vortex structures are observed in the channel with respect to the coarse grid, suggesting the existence of a grid dependency on the size, density, and intensity of the generated vortices. However, one important feature is that even with the coarse grid, vortex structures are clearly seen in the region close to the wall surface (marked in blue). In contrast, having looked at the velocity contours, in the inner layer of LES cases where the roughness exists, the flow seems to change compared with that with a smooth wall. A thicker boundary layer is generated by the effect of the roughness. However, from the top of the rough elements to the center region, the development of turbulence in the streamwise direction seems not significantly influenced by the roughness. Thus, the effect of roughness on the flow field is similar to bringing a rise of the wall boundary by a height related to the size of the rough element that is also seen in the mean streamwise velocity profile in Fig. 5.

From the above discussion, it can be seen that the difference between the results with and without EAT mainly appears in the coarse case, this may be caused by the relatively fine grid resolutions for the present LES cases. To better understand the effect of the EAT, cases with coarser grid resolutions can be tested and compared with that without EAT in a future study. In that case, distortion of roughness configuration by immersed boundary method is thought to be more serious, thus the body fitted grid may be considered more appropriate.

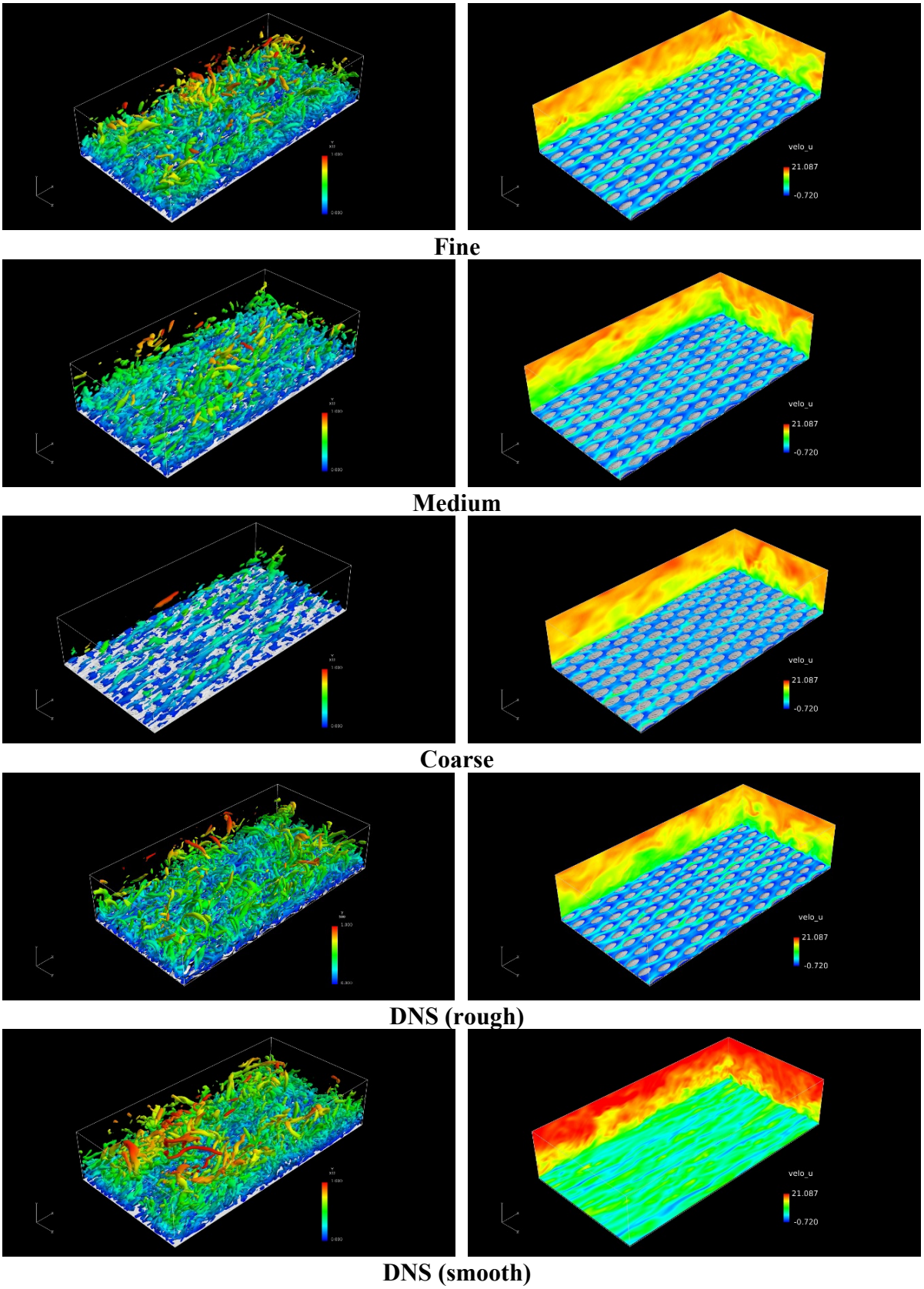

Figure 10: Instantaneous vortex structures and streamwise velocity (4.8, 0.02, 0) contours (with EAT)

To illustrate the reduction of computational cost quantitively, the cost defined by

(Number of grid points $\times$ time step size (which is defined here as $10^{-4}/\Delta t$)) is calculated for the present rough-wall cases and listed in Table 2 with the proportion to the cost of the DNS case. Note that the influence of grid dependency on the convergence time is not considered here. It has to be pointed out that the reduction of computational cost is quite problem that is closely related to the accuracy requirement. Although the cost of the coarse grid is quite lower than that of the fine and medium grids, its prediction accuracy generally decreases. However, considering the fact that the case with EAT yields a better mean velocity profile than that without EAT for the coarse grid, the computational cost of the present model can be even less than that without EAT under a certain accuracy requirement.

Table 2: Computational cost for the rough cases.

	DNS (rough)	Fine	Medium	Coarse
Cost	13414362.5	2663976.3	402712.2	102245
Cost/Cost_DNS	1.0	0.20	0.030	0.0076

5. Conclusions

In this study, LES of turbulent flow in a channel with a rough wall on one side and a free surface on the other was performed by adopting an anisotropy-resolving SGS model. To investigate the grid dependency of the LES results resulting from the SGS model, three grid resolutions were tested under the same definition of a roughness using the immersed boundary method. Obtained results were compared with the corresponding DNS data with and without roughness, as well as the LES results without the extra anisotropic term (EAT).

By comparing the results from smooth and rough DNSs, the presence of roughness caused a downward shift of the mean-velocity profile without any obvious change in slope in the logarithmic law region, which is in line with the general consensus. In addition, from the turbulent stress profiles, there is a shift away from the wall as well as a lower peak value for the streamwise turbulent stress compared with a smooth-wall channel flow.

One main conclusion from the present results is that the grid dependency is not evident for the fine and medium grids in the mean velocity profile as well as turbulence stresses. Some deviation is seen in the mean streamwise velocity profile using the coarse grid. This may be partly a result of reproducing wall roughness using the immersed boundary method, as the rough surface is modified to a height that is slightly lower because the steps were relatively larger. As for the turbulent stresses, the grid dependency seems to bring a non-negligible influence. The vortex structures are also shown to be affected in size, distribution or intensity to some extent, depending on the grid resolution used. Further detailed investigation will be necessary on this issue.

In this study, simulations without the EAT were also performed and their results were compared with those using the anisotropy-resolving SGS model (with EAT). By comparing the results with and without EAT, the mean velocity profile and turbulent stresses agree relatively well for the fine and medium grid cases, whereas for the coarse grid case, the EAT plays a more important role, bringing about a larger difference in prediction accuracy. The present SGS model with EAT successfully provides the predictions of the mean velocity and the Reynolds shear stress better than the model without EAT does. This indicates that the model with EAT

can considerably reduce the grid dependency for coarse grid resolutions. Concerning the Reynolds normal stresses, on the other hand, lower values are yielded by the model with EAT compared with those by the model without EAT. Particularly, a remarkable difference is seen in the wall-normal component. In fact, however, this is caused mainly by the effect of the isotropic SGS stress distribution predicted by the model without EAT, where the wrong wall-limiting behavior gives considerably higher wall-normal SGS component. From these results, it has been confirmed that the present SGS model with EAT is useful for application to turbulent flows with wall roughness, although further discussion is necessary to improve the model performance.

Acknowledgements

This research was partially supported by Grant-in-Aid for Scientific Research 16K05042, sponsored by the Japan Society for the Promotion of Science. This work was also supported by the 'Advanced Computational Scientific Program' of the Research Institute for Information Technology, Kyushu University, Japan. The computation was performed mainly using the computer facilities at the Research Institute for Information Technology, Kyushu University, Japan. YZ was financially supported by the China Scholarship Council.

References

1. D. Chatzikyriakou, J. Buongiorno, D. Caviezel, D. Lakehal. DNS and LES of turbulent flow in a closed channel featuring a pattern of hemispherical roughness elements. *International Journal of Heat and Fluid Flow*. 2015; 53: 29-43.
2. K. Bhaganagar, J. Kim, G. Coleman. Effect of Roughness on Wall-Bounded Turbulence. *Flow, Turbulence and Combustion*. 2004; 72: 463-492.
3. Hamid Shamloo, Bahareh Pirzadeh. Analysis of roughness density and flow submergence effects on turbulence flow characteristics in open channels using a large eddy simulation. *Applied Mathematical Modelling*. 2015; 39: 1074-1086.
4. Y. Jin, M.F. Uth, H. Herwig. Structure of a turbulent flow through plane channels with smooth and rough walls: An analysis based on high resolution DNS results. *Computers & Fluids*. 2015; 107: 77-88.
5. M. D. Marchis, E. Napoli. Effects of irregular two-dimensional and three-dimensional surface roughness in turbulent channel flows. *International Journal of Heat and Fluid Flow*. 2012; 36: 7-17.
6. A. G. Andersson, J. Gunnar, I. Hellström, P. Andreasson, T. S. Lundström. Effect of spatial resolution of rough surfaces on numerically computed flow fields with application to hydraulic engineering. *Engineering Applications of Computational Fluid Mechanics*. 2014; *Vol*. 8, No. 3, *pp*. 373-381.
7. J. Bailon-Cuba, S. Leonardi, L. Castillo. Turbulent channel flow with 2D wedges of random height on one wall. *International Journal of Heat and Fluid Flow*. 2009; 30: 1007-1015.
8. S. Leonardi, I., P. Castro. Channel flow over large cube roughness: a direct numerical simulation study. *J. Fluid Mech*. 2010; *vol*. 651, *pp*. 519-539. Cambridge University Press 2010.
9. Y. Nagano, H. Hattori, T. Houra. DNS of velocity and thermal fields in turbulent channel flow with transverse-rib roughness. *International Journal of Heat and Fluid Flow*. 2004; 25: 393-403.

10. J.M. Tsikata, M.F. Tachie. Adverse pressure gradient turbulent flows over rough walls. *International Journal of Heat and Fluid Flow*. 2013; 39: 127-145.
11. M. P. Schultz, K. A. Flack. The rough-wall turbulent boundary layer from the hydraulically smooth to the fully rough regime. *J. Fluid Mech.* 2007; *vol. 580, pp. 381-405.* Cambridge University Press, 2007.
12. L. Keirsbulck, A. Mazouz, L. Labraga, C. Tournier. Influence of the surface roughness on the third-order moments of velocity fluctuations. *Experiments in Fluids*. 2001; 30: 592-594.
13. P.-Å. Krogstad, R. A. Antonia. Surface roughness effects in turbulent boundary layers. *Experiments in Fluids*. 1999; 27: 450-460.
14. J. Smagorinsky. General circulation experiments with the primitive equations. I. The basic experiment. Mon. *Weather Rev*. 1963; 91, 99
15. M. Germano, U. Piomelli, P. Moin, W. H. Cabot. A dynamic subgrid-scale eddy viscosity model. *Phys. Fluids* A 3 (7). 1991; 1760-1765.
16. D. K. Lilly. A proposed modification of the Germano subgrid-scale closure method. *Phys. Fluids* A 4 (3). 1992; 633-635.
17. Y. Zang, L. Robert. Street, and Jeffrey R. Koseff. A dynamic mixed subgrid-scale model and its application to turbulent recirculating flows. *Phys. Fluids* A 5 (12). 1993; 3186-3196.
18. J. Bardina, J. H. Ferziger, and W. C. Reynolds. Improved turbulence models based on large eddy simulation of homogeneous, incompressible, turbulent flows. Ph. D. dissertation, Department of Mechanical Engineering, Stanford University, 1983.
19. B. Vreman, B. Geurts, H. Kuerten. On the formulation of the dynamic mixed subgrid-scale model. *Phys. Fluids* 6 (12). 1994; 4057-4059.
20. K. Abe. An improved anisotropy-resolving subgrid-scale model with the aid of a scale-similarity modeling concept. *International Journal of Heat and Fluid Flow*. 2013; 39: 42-52.
21. J. Bardina, J. H. Ferziger, W. C. Reynolds. Improved subgrid scale models for large eddy simulation. AIAA Paper. 1980; 80-1357.
22. R. D. Moser, J. Kim, N. N. Mansour., Direct numerical simulation of turbulent channel flow up to $Re_\tau = 590$. *Physics of Fluids*. 1999; 11: 943-945.
23. T. Hirose, H. Kihara, K. Abe. Numerical simulation of flow field around a wing with surface oscillation using an immersed boundary method, The 90th conference of JSME fluid dynamics division, CD-ROM, 2012.
24. D. Chung, L. Chan, M. MacDonald, N. Hutchins, A. Ooi. A fast direct numerical simulation method for characterising hydraulic roughness. *J. Fluid Mech*. 2015, vol. 773, pp. 418-431.
25. http://www.ciss.iis.u-tokyo.ac.jp/rss21/.
26. K. Abe. An investigation of SGS-stress anisotropy modeling in complex turbulent flow fields. *Flow, Turbulence and Combustion*. 2014; 92: 503-525.